ACS APPLIED MATERIALS & INTERFACES

Research Article

www.acsami.org

Synthesis of High Saturation Magnetization Superparamagnetic Fe_3O_4 Hollow Microspheres for Swift Chromium Removal

Yubiao Liu,[†] Yongqiang Wang,[†] Shaomin Zhou,*[,†] Shiyun Lou,[†] Lin Yuan,[‡] Tao Gao,[†] Xiaoping Wu,[†] Xiaojing Shi,[†] and Ke Wang[†]

[†]Key Lab for Special Functional Materials of Ministry of Education, Henan University, Kaifeng 475004, People's Republic of China

[‡]Department of Biology and Chemistry, Hunan University of Science and Engineering, Yongzhou Hunan 425100

Supporting Information

ABSTRACT: High saturation magnetization monodisperse Fe_3O_4 hollow microspheres (109.48 emu/g) with superparamagnetic property at room temperature are promptly synthesized by a one-step solvothermal process with the presence of sodium dodecylbenzenesulfonate as an additive. The as-synthesized products possess superparamagnetism, large cavity, high water solubility, and saturation magnetization at room temperature. In particular, these hollow microspheres exhibit both of a rather short separation time from industry wastewater and a high adsorption capacity about 180 mg/g at high Cr(VI) concentrations, which is much better than those of reported magnetite solid nanoparticles. In addition, the X-ray photoelectron spectra (XPS) show that the uptake of Cr(VI) into the spheres was mainly governed by a physicochemical process. The micelle-assisted Ostwald ripening process was proposed to explain the rapid formation of hollow structures by a series of control experiments. The as-manufactured products with the two advantages mentioned above serve as ideal candidates for environmental remediation materials.

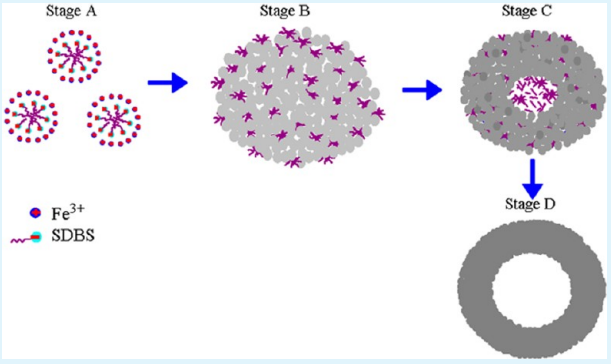

KEYWORDS: *superparamagnetism, magnetite, high saturation magnetization, fast chromium removal, water treatment, adsorption*

INTRODUCTION

Cr (VI) is generally considered to pose great human health risk because it is more toxic, soluble and mobile than Cr (III),[1,2] and has become one of the most frequently detected groundwater at hazardous waste sites. Therefore, considerable attention has been paid to the treatment of industry wastewater containing Cr (VI) over the past few decades, and a variety of methods have been developed for the removal of Cr(VI) from wastewater.[3−6] Among these methods, chemical reduction followed by adsorption is the most widely used technique,[7] in which Cr(VI) is converted into trivalent chromium (Cr(III)) with much lower toxicity and limited hydroxide solubility, and magnetite that can be subsided under a magnetic field has been a promising reducing agent in the field of chromium ion removal lately.[3,7]

To improve the practical application prospects of the magnetite, as an important parameter, the separation time of the magnetite from the solution has to be shortened.[8−13] It is sure that the magnetite with a high saturation magnetization promises rapid separation of the Cr from the wastewater by an external magnetic field.[9] Compared with pure bulk magnetic materials, however, the magnetism of small magnetic nanoparticles (NPs) or nonmagnetic coated nanostructures is weaker, which can make the separation of the magnetite from the solution prolonged.Two techniques (adding some high saturation magnetization compositions[9] and preparation of secondary nanostructures[10,14−16]) to solve this problem have therefore been focused on the preparation of high saturation magnetization (M_S) magnetite nanostructures. For example, Zhu et al.[9] reported a large M_S (96.3 emu/g) of the synthesized nanoparticles for fast chromium removal by increasing Fe core. Unfortunately, there is a complex structure in their products in which it is difficult to fabricate this product. In fact, creation of secondary nanostructures with the microsphere characteristics can retain a M_S as high as the counterpart bulk material although the nanostructure does not lead to a magnetization enhancement.[14−16] In addition, in order to combine the individual NPs with the possibility to tune collective properties and control them, manipulation of the secondary structures of NPs is desired, although the magnetization depends on the magnetic moments of the particles per volume unit and there is no relation with the final magnetic collective system.[14−16] In particular, the approach of forming large complex structures of NPs appears more attractive because the proportion of atoms located in the surface increases and these atoms are hardly to reverse with the magnetic field, the shape of the hysteresis loop

Received: July 5, 2012
Accepted: August 20, 2012
Published: August 20, 2012

is changed, and microsphere characteristics occur and a final M_S is as high as the counterpart bulk.[14−16]

More recently, our group[2] has reported that Fe_3O_4/polypyrrole (PPy) composite microspheres have a strong adsorption capability (~209.2 mg/g). However, the synthesized products possess a low saturation magnetization (25.06 emu/g), which makes it difficult to rapidly separate from wastewater by an external magnetic field although compared with nonmagnetic nanostructure, it is easy to separate from wastewater.[2] Previously, we[16] reported the fabrication of superparamagnetic Fe_3O_4/PVP nanocomposite hollow microspheres with a high saturation magnetization by PVP as an additive. In this study, based on a similar way, monodisperse magnetite hollow spheres are obtained by sodium dodecylbenzenesulfonate (SDBS) as an additive in which the as-fabricated samples with higher high saturation magnetization are more simple, economical and environmentally benign method via a micelles-assisted one-pot reaction. In addition, a plausible formation mechanism has been proposed based on a systematic investigation of the assembly process. By controlling the concentration of SDBS, the structure of the products can be tailored from solid spheres to hollow ones. In particular, the magnetic, chromium ion absorption, and separating properties were investigated.

EXPERIMENTAL SECTION

Materials. Ferric chloride hexahydrate ($FeCl_3·6H_2O$), sodium dodecyl benzene sulfonate (SDBS), sodium acetate (NaAc), potassium dichromate ($K_2Cr_2O_7$) and ethylene glycol (EG) were purchased from Sinopharm Chemical Reagent Co., Ltd. All reactants were of analytical grade and used as received without any further purification.

Polymerization Procedure. In a typical experiment, first, 0.16 g (0.46 mmol) of SDBS surfactant in EG (16 mL) was stirred vigorously at room temperature to give a transparent solution. Next, 0.54 g (2 mmol) of $FeCl_3·6H_2O$ and 0.93 g o fNaAc (11 mmol) were added to the surfactant solution with vigorous stirring. After addition, the solution was transferred into a Teflon-lined stainless-steel autoclave with volume of 25 mL, and subsequently sealed and heated at 453 K for 12 h in an oven. The black product was centrifuged and washed with deionized water and ethanol three times and then dried under vacuum overnight for further characterization. In the synthesis process, SDBS forms micelles in solution, which promotes the formation of nuclei near the micelles surface, and dexterously accelerates the formation of the hollow spheres. To investigate the formation mechanism of the hollow magnetite microspheres, we carried out a series of experiments, varying the reaction time and the amount of SDBS added.

Characterization. Samples dispersed at an appropriate concentration were respectively cast onto a conductive adhesive and a carbon-coated copper grid at room temperature for characterization of scanning and transmission electron microscopy (SEM and TEM). SEM, TEM, and high-resolution TEM (HRTM) images were performed using a JSM 5600LV, a JEM-100CX II, and a JEM-2010 (all from JEOL, Japan), respectively. X-ray diffraction (XRD) patterns were obtained using the X'Pert Pro (Philips, Netherlands). X-ray photoelectron spectroscope (XPS) was recorded on an AXIS ULTRA. The magnetic measurements were recorded by a superconducting quantum interference devices magnetometer (SQUID, MPMS XL7, USA). The samples were dried and mixed with KBr to be compressed to a plate for Fourier transform infrared (FT−IR) measurement. FT−IR spectra were recorded on the Thermo Nicolet Avatar 360 FTIR Spectrometer (Thermo Nicolet Corporation, Madison, Wisconsin, USA).

Adsorption Experiments. $K_2Cr_2O_7$ was used as the source of Cr (VI). The different concentrations of Cr(VI) ions were prepared and the pH value of 2.5 was adjusted by HCl or NaOH. For each sample, 10 mg adsorbent was dispersed into the above solution (40 mL), and then kept for 12 h to establish adsorption equilibrium at room temperature. The adsorbent was then separated from the mixture by a permanent magnet (0.05 T). To determine Cr (VI) ions removal by the adsorbent, the Cr(VI) concentration in the remaining solution was measured by an inductively coupled plasma atomic emission spectrophotometer (PE2400-II, PerkinElmer, USA).

RESULTS AND DISCUSSION

Characterizations. Phase structure and composition of the sample obtained in a typical synthesis were identified by XRD and XPS. A typical XRD pattern of the as-obtained sample is shown in Figure 1. It is found that all the diffraction peaks can

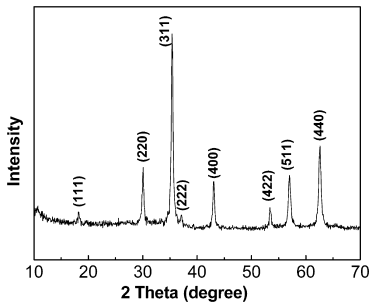

Figure 1. XRD pattern of the obtained Fe_3O_4 hollow microspheres.

be well indexed to the magnetic cubic structure of Fe_3O_4 (JCPDS 79−0419). In addition, there are not typical γ-Fe_2O_3 (JCPDS Card No. 39−1346) peaks such as (210) and (211), indicating the absence of γ-Fe_2O_3. As shown in Figure S1 (please see the Supporting Information), the X-ray photoelectron spectrum (XPS) of the sample obtained exhibits peaks at 710.5 and 724.1 eV, which are the characteristic peaks of Fe 2p3/2 and Fe 2p1/2 oxidation states, respectively.[7,17,18] There are no obvious shakeup satellite structures at the higher binding energy side of both main peaks, which is the characteristic of Fe_3O_4. Completely removing of SDBS is confirmed by Fourier transform infrared (FT-IR) spectroscopy as shown in Figure S2 in the Supporting Information. The peaks appearing at 581 and 415 cm^{-1}, attributed to the typical band of Fe_3O_4, correspond to the stretching vibration modes of Fe−O.[18] The spectral features of standard SDBS show bands between 3100 to 3000 cm^{-1} and many intense and sharp bands in the range 1600 to 1450 cm^{-1} corresponding to benzene ring skeleton vibration and C−H stretching of aromatic ring. Absence from the FT-IR spectral features of the synthesized products confirms the complete removal of the SDBS from the pores of the magnetite hollow spheres. XRD, XPS, and FT-IR results demonstrate that the pure magnetite hollow spheres have been successfully synthesized by this facile and flexible route.

The morphologies and sizes of the typical samples were examined by SEM and TEM. The SEM image (Figure 2a) shows that the product consists of a larger quantity of well-dispersed spherelike shapes and the size distribution of the spheres is narrow. From the TEM image (Figure 2b), we can observe that each of the spheres has a pale center region in contrast to a dark edge, suggesting all spheres are hollow structures with ~450 nm in diameter and 110 nm in shell thickness, respectively. In a word, the SEM and TEM images together confirm that the as synthesized products are uniform hollow spheres. It should be noted that the hollow spheres with narrow size distribution are well dispersed. More detailed structural information of synthesized products was provided by

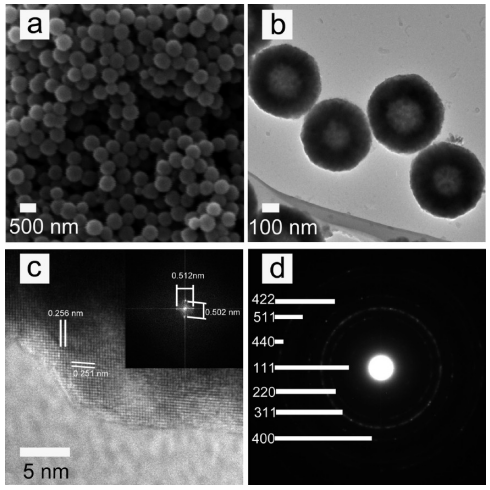

Figure 2. As-synthesized Fe_3O_4 hollow microspheres of (a) SEM, (b) TEM, (c) HRTEM image and its FFT image (inset), and (d) SAED patterns.

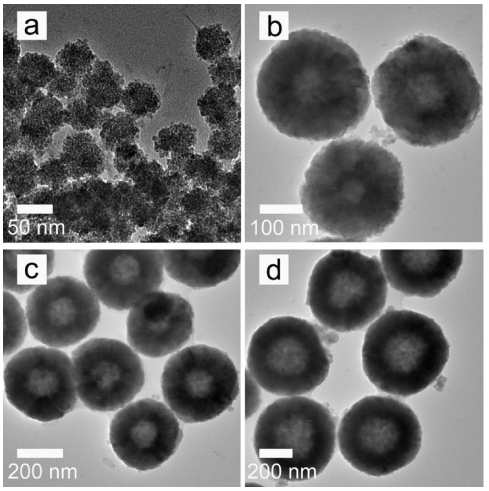

Figure 3. TEM images of products synthesized at different reaction times: (a) 3, (b) 6, (c) 9, and (d) 15 h. Other conditions were the same as the typical synthesis.

the HRTEM analysis. The HRTEM image (Figure 2c) shows well-defined 2D lattice planes and demonstrates the good crystallinity of nanoparticle. Correspondingly, the Fast Fourier Transition (FFT) pattern (inset in Figure 2c) shows obvious single-crystalline nature and can be easily indexed to the cubic structure. In agreement with the measurement in the FFT image, the lattice planes with *d*-spacing of 0.256 and 0.251 nm correspond to (311) and $(11\bar{3})$ planes, respectively. SAED (Figure 2d) taken from the edge of a Fe_3O_4 hollow sphere shows polycrystalline diffraction, suggesting that it consists of many Fe_3O_4 NPs. From inside to outside, the rings can be indexed to (111), (2 2 0), (3 1 1), (4 0 0), (422), (5 1 1), and (4 4 0) planes of spinel Fe_3O_4, respectively.

To investigate the formation mechanism of the hollow structured magnetite spheres, we carried out a series of experiments. The results show that the temperature, time, the amount of SDBS play key roles in the formation of monodisperse Fe_3O_4 hollow spheres. When the temperature decreases to 160 °C, only brown precipitates, instead of black Fe_3O_4, are obtained after reaction for 12 h, which is the same as the products synthesized at 180 °C for 2 h. However, if the temperature is too high (up to 200 °C), the hollow microspheres with a broad diameter distribution are synthesized. It was experimentally confirmed that although ethylene glycol (EG) is an excellent reducing agent with a relatively high boiling point (471 K), which provides a rather mild reducing environment in the solvothermal process,[19−22] no resulting products were obtained under the same experiment conditions without NaAc which acted as a mild precipitator and provided an alkaline atmosphere for the solution system.[23−26]

To investigate the evolution process of the core evacuation, time-dependent experiments were conducted. After 2 h hydrothermal treatment, no precipitation was obtained except for orange suspension. When proceed for 3 h, only a small part of the orange suspension transform into black precipitate. There was no obvious peak found on the XRD pattern of the product (see Figure S3a in the Supporting Information). From the TEM image of the black precipitate, we found that the sieve-like clusters were assembled by many spherical aggregates with pore size of about 3−4 nm (Figure 3a). Increasing the reaction time to 6 h, all of the orange suspensions transform into black precipitate. The peaks belonged to spinel Fe_3O_4 appeared on the XRD pattern of the black precipitation (see Figure S3b in the Supporting Information), implying the start of crystallization. As shown in Figure 3b, the black precipitate consisted of monodisperse hollow spheres with an average diameter of 260 nm and a shell thickness of 80 nm. Further prolonging the reaction time to 9 h, the crystallinity of the product was increased (see Figure S3c in the Supporting Information). Meanwhile, it can be observed that the diameters of the hollow spheres were increased to 350 nm and the inner space of the spheres was further increased in comparison to the shell (Figure 3c). As the reaction time went on to 15 h, the products were completely transformed into well-crystallized hollow spheres (see Figure S3d in the Supporting Information). The diameters and cavity of the hollow spheres are further increased (Figure 3d), indicating continued evacuation of central cavities. To sum up, with the proceeding of the reaction, the sievelike clusters began to gather fused into a large hollow sphere which was gradually converted to well-crystallized hollow sphere and the diameter and cavity of the hollow sphere had a tendency to increase until complete crystallization of hollow spheres.

Although the hollowing process could be well explained by Ostwald ripening, it is noted that the time needed to form hollow structures in our process using SDBS is much shorter and the hollow interior is much more distinct than that of previous reported.[27,28] These results reveal that the core evacuation could occur using different surfactants in EG system,[24,27,28] but the hollowing effect is distinguishing for different surfactants with the same reaction time, and the hollowing process could be significantly accelerated with the assistance of SDBS as the surfactant. SDBS, a kind of anionic surfactant, has been used as stabilizer to modify Fe_3O_4 nanoparticles.[29,30] Like other amphiphilic surfactants,[18,31] it can also form micelles when SDBS reaches a certain concentration in the solution.[31,32] According to previous reports,[33,34] to determine the ability to form SDBS micelles in the media of EG, we carried out UV−visible experiments of the different SDBS concentrations in the EG solution. As shown in Figure S4 in the Supporting Information, based on the UV−visible absorption spectrum, an absorption peak caused by SDBS micelles appears in the 326 nm. Therefore, in a typical synthesis condition, SDBS in the EG solution can

form micelles. The surface of SDBS micelles with negative charge attracts positive charge iron ions due to electrostatic attraction, which is in favor of the initial nanocrystalline nucleate near in micelle surface. Meanwhile, the fresh produced micelles have high surface energy due to their small diameter (high curvature) and provide the heterogeneous nucleation center for newly formed nanoparticles to aggregate around the micelles.[24] The spherical aggregates are then formed and thus the SDBS was remaining in the interior of the aggregates. Figure 4 gives a representative high-magnification TEM image

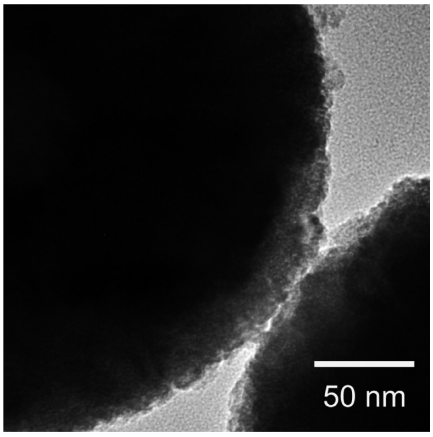

Figure 4. Representative high-magnification TEM image of spherical aggregate synthesized at 180 °C for 6 h.

of spherical aggregate synthesized at 180 °C for 6 h, which indicates that the aggregates are constructed of many small nanocrystals and wormlike nanopores with pore size of several nanometers, can be seen clearly in the nanocrystallites forming the spherical loose nanostructures. The wormlike nanopores are suggested to be evidence of micelles in the aggregates. Since the original driving force for this ripening could be attributed to the intrinsic density variations inside the starting solid aggregates, the loosely packed crystallites in the shell would serve as starting growth sites for the subsequent recrystallization and speed up the mass transport.[24] During the ripening process, the smaller crystallites located at central cores tend to relocate themselves to the shell, and the interior space continues to expand. The inner nanospace occupied by the micelles is released and becomes part of the void space. As a result, the distinctly hollowing effect could be observed in a short reaction time.

As indicated in above investigations, it is suggestive that Ostwald ripening is also associated with the SDBS micelles in the solution during the synthesis. This point is further addressed in the following synthetic experiments. With other synthetic conditions held constant, adjusting the concentration of SDBS led to an obvious shape evolution of Fe_3O_4 particles from solid microspheres to hollow microspheres, and large microspheres as shown in Figure 5. It has been proven that the morphology of the surfactant micelles may range from spherical shape to prolate or rodlike, and lamellar phase, which can be dramatically affected by its concentration, thus resulting in the obvious evolution of the shape of inorganic crystals.[30,31] When the concentrations of SDBS are 0 M and 0.72 mM, the Fe_3O_4 nanocrystals began to exhibit a strong tendency to assemble into large particles under the experimental conditions and solid spheres that resulted from the assembly of nanoparticles were

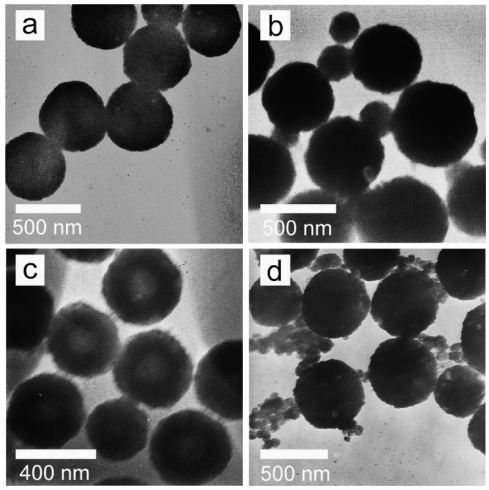

Figure 5. TEM images of products synthesized with the SDBS concentration of (a) 0, (b) 0.72, (c) 14.3, and (d) 43.2 mM.

obtained (Figure 5a, b). Compared to the hollow spheres prepared under the typical conditions (SDBS: 28.7 mM), when the concentration of SDBS increases to 14.3 m M as shown in Figure 5c, no significant morphology change appears. Further increasing the concentration of SDBS to 43 mM, the nanoparticles tend to assemble into even large solid spheres (Figure 5d).

Formation Mechanism. On the basis of above investigations, a proposed mechanism for micelles-assisted synthesis of magnetite hollow spheres is schematically illustrated in Figure 6. SDBS, which reaches a certain concentration in

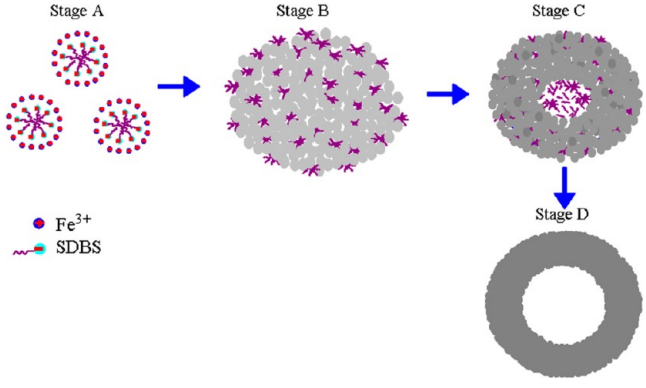

Figure 6. Schematic illustration of the process of obtaining magnetite hollow microspheres.

solution, can form spherical micelle and attracts iron ions with positive charge due to electrostatic attraction in the EG solvent (stage A). Then, original nanocrystallites nucleate near the interface of micelles and spontaneously aggregated to form the large spherical clusters in the EG solvent due to the strong surface tension (stage B). In this process, surface hydroxyl groups in the surfactant coordinate with primary magnetite nanoparticles in EG solvent, showing that the micelles play a crucial role in the formation of spherical morphology.[18] The micelles were used as pore-forming template, and the wormhole-like porosity is due to the interparticle connections between agglomerated nanocrystals. With the continuation of the reaction time, the crystallites located in the inner cores are easily dissolved duo to the higher surface energies compared to

those in the outer surfaces. Thus, the subsequent crystallization process occurred using the nanocrystallites located in the shell as nucleation seeds, which leads to the durative growth of the shell at the expense of the cores inner spheres, and the results of this process are that the size of the core is reduced gradually while the hollow volume is enlarged (stage C). Finally, the hollow microspheres are formed with the complete depletion of the cores after washing (stage D). Considering the inner space occupied by the micelles, this solid evacuation process is faster than the general symmetric ripening.

Magnetic Properties. Figure 7 displays the magnetization curves measured at 300 K in the applied magnetic field

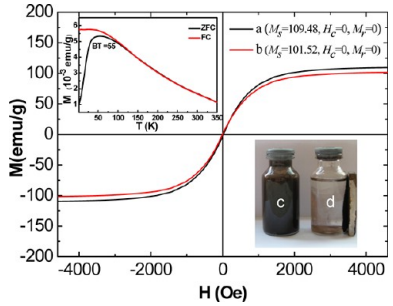

Figure 7. Room-temperature magnetization curves for the typical Fe_3O_4 hollow microspheres (a) before adsorption and (b) after adsorption; photographs of magnetite hollow spheres dispersion in a vial: (c) without magnetic field and (d) with magnetic field for 0.5 min. The inset at the top shows ZFC and FC curves of the typical Fe_3O_4 hollow microspheres measured with the field of 500 Oe.

sweeping from −4.5 to 4.5 kOe for the typical Fe_3O_4 hollow spheres before and after adsorption. The curves (Figure 7a, b) show no remnant magnetization or coercivity, indicating that both samples may be superparamagnetic at room temperature. The inset at the top is the temperature dependence of the magnetization for field-cooled (FC) and zero-field-cooled (ZFC) Fe_3O_4 hollow spheres before adsorption under an applied magnetic field of 500 Oe. Similar to previous reports,[16,35] The FC and ZFC magnetization curves are split below blocking temperature (TB, about 55 K) and overlap with each other above TB as the remanence and coercivity have vanished, which confirms that the sample is superparamagnetic behavior at room temperature. It is noted that the saturation magnetization (Ms) values (109.48 emu/g) of Fe_3O_4 hollow spheres before adsorption exceeds the Ms value of the reported nano/microscale magnetite spheres.[16,24,36] The larger diameter (~450 nm) may be the reason of the higher Ms value, compared to our previous synthesis of Fe_3O_4 hollow spheres (~ 250 nm of diameter).[15,16] In addition, the structure of the particle in the hollow microspheres is an important factor for the properties of magnetization.[24,30] Previous studies have shown that the saturation magnetization of the particle could be affected by their structure, such as defects, size, crystalline, and coupling.[24,35] As shown in Figure 1, the nanoparticles with a high-quality crystallinity are confirmed by XRD characterization. The primary high-quality-crystalline nanoparticles lead to hollow microspheres with magnetic properties superior to the individual nanoparticle and improved coalescence of the crystallites in the secondary structures where each of them is composed of primary nanoparticles results in increased magnetic coupling and higher magnetization.[15,16] Below a certain critical size, the primary magnetic particles become single domain instead of an usual multidomain structure of the bulk magnetic materials.[16] Therefore, the hollow spheres exhibit superparamagnetic properties. The SDBS has been cleaned from the surface of the nanoparticles, which have been confirmed by the FT-IR test (see Figure S2 in the Supporting Information), and there is no magnetically dead or antiferromagnetic layer on the outside of the products, which would lead to a decrease in M_s.[23] Moreover, Figure 2c confirms that there is less crystal defects in nanoparticles. Therefore, the better properties of magnetization for the synthesis Fe_3O_4 hollow spheres are more likely attributed to their primary particles which have good crystallinity, less crystal defects, and increasing coupling.[16,23,24] The use of additives on the magnetic properties is also very important, which may affect the size of the hollow spheres and the structure of the primary particles, such as defects, size, and coupling,[30,37−39] and it can be speculated that the SDBS play a key role on improving the properties of magnetization. The exact mechanism for the relationship between the structure of primary nanoparticles and the additive is worthy of further investigation. Slight agitation can bring the hollow spheres to back into the aqueous solution when the magnet is removed (Figure 7c) although these magnetic hollow spheres can be completely separated from the solution when the solution is subjected to an external magnetic field within minute, as shown in Figure 7d. It can be obviously seen that the obtained Fe_3O_4 hollow spheres have rapid magnetic response ability at room temperature, as well as, highly monodispersed, and water-soluble.

Isotherms and Kinetics of the Cr (VI) Adsorption. The magnetite is an effective reducing agent for the treatment of Cr (VI),[7] and the hollow spherical structure is usually employed for wastewater treatment because of its capability to adsorb a large quantity of pollutants, and/or high efficiency in degrading the unwanted species.[40,41] In this case, the obtained typical Fe_3O_4 hollow microspheres were investigated for the treatment of Cr (VI) at room temperature (300 K) based on the above characterization. The detailed relationship between the removal ability and the concentration of the Cr (VI) ions solution can be illustrated by an adsorption isotherm.

The Langmuir and Freundlich isotherm models are applied to simulate Cr (VI) adsorption on Fe_3O_4 hollow microspheres. The Langmuir model is expressed as

$$Q_e = bQ_mC_e/(1 + bC_e) \quad (1)$$

The Freundlich isotherm model can be expressed by the following formula

$$Q_e = kC_e^{1/n} \quad (2)$$

where C_e is the equilibrium concentration of Cr (VI) in the supernatant (mg/L); Q_e is the amount of Cr (VI) adsorbed on per weight of magnetite hollow microspheres (mg/g) after adsorption equilibrium; Q_m represents the maximum adsorption capacity of Cr (VI) on per weight of Fe_3O_4 hollow microspheres (mg/g); and b is the Langmuir adsorption constant (L/mg). The Freundlich constant k is correlated to the relative adsorption capacity of the adsorbent (mg/g), and $1/n$ is the adsorption intensity.

Figure 8 shows the adsorption isotherm of Cr (VI) for the as-prepared magnetite hollow microspheres. The adsorption isotherm appeared to consist of two Langmuir or Freundlich isotherm for Cr (VI). The experimental data are simulated with the Langmuir isotherm models and Freundlich isotherm

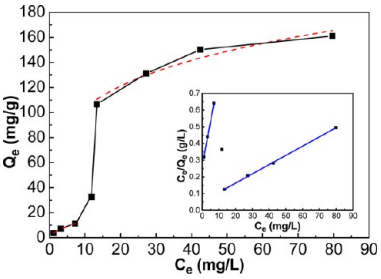

Figure 8. Cr (VI) adsorption isotherm of typical Fe_3O_4 hollow microspheres and (inset) C_e/Q_e versus C_e plot. Blue solid and red dotted lines are the Langmuir and Freundlich model of the analog line, respectively.

models, respectively. The relative parameters calculated from the models are listed in Table S1 in the Supporting Information. At low initial concentrations (<10 mg/L Cr (VI)), the higher correlation coefficient of the Freundlich model indicates that the adsorption data are better fitted by the Freundlich model (R^2 = 0.996) rather than by the Langmuir model (R^2 = 0.985). The calculated values of Q_m are 17.98 mg/g for Fe_3O_4 hollow microspheres, which is close to the previously magnetite particles.[3] At initial Cr (VI) concentration of 20 mg/L, the adsorption data deviate from the simple Langmuir isotherm and at high initial Cr (VI) concentrations (>40 mg/L Cr (VI)), the adsorption data follow a second Langmuir or Freundlich isotherm. the higher correlation coefficient of the Langmuir model also indicates that the adsorption data are better fitted by the Langmuir model (R^2 = 0.999) rather than by the Freundlich model (R^2 = 0.928). The second maximum adsorption capacities (Q_m) for Cr(VI) were substantially higher (180 mg/g), which is much higher than the previously magnetite or surface-modified magnetite particles.[3,42] The adsorption experimental result is stable, and based on several tests, the error limits of the adsorption capacity are less than 7% and 2% (see Table S2 in the Supporting Information) at low concentrations and high concentrations, respectively. It is noteworthy that a biphasic behavior for Cr (VI) sorption is especially obvious and similar adsorption characteristics have been reported in magnetite partials for the As (V) and As (III) adsorption due to the surface complexation.[43,44] The biphasic behavior of the characteristic and high adsorption capacity for Cr (VI) sorption on the magnetite hollow microspheres may be a result of the surface complexation of Cr with Fe on the surface and the secondary hollow nanostructure, which provides an accessible diffusion pathway into the interior of Fe_3O_4 hollow microspheres.

The adsorption of the Cr (VI) with different concentrations onto Fe_3O_4 hollow microspheres was also investigated as a function of contact time at room temperature with solution pH value 2.5. For example, when 20 mg of as-prepared Fe_3O_4 hollow microspheres was dispersed into 20 mL of Cr (VI) solution with concentrations of 10 and 80 mg/L, more than 67% and 90% of the Cr (VI) in the solution could be removed in less than 30 min, as illustrated in Figure S5 in the Supporting Information. After adsorption, the Cr (VI)-loaded magnetite hollow spheres can be rapidly separated from the solution at an appropriate external magnetic field due to their high saturation magnetization (101.52 emu/g, Figure 7 b), while the separation of weakly magnetic adsorbent from the solution is very slow at the same external magnetic field. The rapid separation characteristic of adsorbent is of practical significance for its industrial applications.

Adsorption Mechanisms and Regeneration Tests. To investigate the adsorption mechanism of the magnetite hollow spheres for Cr(VI) removal, both XRD and XPS techniques were used to characterize the adsorbent surface after Cr (VI) adsorption (pH 2.5; initial Cr (VI) concentration 50 mg/L; 12 h). The Cr2p XPS spectra of the adsorbent exhibit two peaks centered at 575.6 and 585.5 eV (see Figure S6b in the Supporting Information), assigned to Cr2p3/2 and Cr2p1/2, respectively. These peaks are typically ascribed to Cr (III), indicating that the Cr (VI) in solution had been adsorbed onto the surface of the adsorbents and then reduced to Cr (III) by a redox process.[7,17] Fe2p XPS spectra show only fully oxidized iron on the surface due to characteristic of the 2p3/2 peaks centered at ca. 711.1 eV see (see Figure S6c in the Supporting Information).[7,17] However, in the Fe2p XPS spectra of magnetite before adsorption (see Figure S1 in the Supporting Information), the 2p3/2 peak is centered at ca. 710.5 eV, which matches well with the data of referenced magnetite. The XRD pattern of adsorbent (see Figure S6d in the Supporting Information) should be assigned to the pattern of maghemite rather than magnetite, although both of the phases have spinel-type structure and exhibit very similar XRD patterns. This assignment is supported by the XPS result that adsorbent shows a fully oxidized state. These above results indicate that the magnetite was oxidized into maghemite during the adsorption of Cr (VI), and the resulting Cr (III) species exist in the surface of the adsorbent.

A simple regeneration test was conducted to evaluate the cycle properties of the Cr (V) absorption for the synthesized Fe_3O_4 hollow microspheres. The testing process followed a typical route proposed by Yuan et al.[7] Typically, NaOH solution (0.01M) was used to remove the adsorbed Cr (VI) ions. For example, 20 mg of the as-prepared Fe_3O_4 hollow microspheres was dispersed into 20 mL of Cr (VI) solution with concentrations of 10 and 80 mg/L, respectively. The restored Cr (VI) adsorption capacity of Cr(VI)-loaded magnetite hollow spheres obtained by initial Cr(VI) solution with concentration of 10 mg/L was found to be 45.1, 20.5, and 9.7% of the original adsorption capacity of sample, corresponding to the three cycles, respectively, and the values with same meaning for Cr (VI)-loaded magnetite hollow spheres obtained by initial Cr (VI) solution with concentration of 80 mg/L were 25.8, 7.6, and 3.3%, respectively. These results show that the regeneration of Fe_3O_4 hollow spheres was much less efficient than that of the maghemite nanoparticles, whose Cr adsorption capacity remained almost constant even after six cycles of elution/adsorption.[45] This is due to that Cr(VI) adsorption onto maghemite was a reversibly physical process, that is electrostatic attraction. On the contrary, the irreversible redox and the electrostatic attraction occurred in the process of Cr (VI) adsorption on magnetite nanoparticles.[3,7] It is clear that the adsorption and reduction ability of magnetite hollow spheres for Cr (VI) is affected by Cr (VI) concentration, and other detailed studies are needed in the future work.

CONCLUSION

In summary, we demonstrate a novel and facile synthetic route for the synthesis of magnetite hollow microspheres. Investigation of the formation mechanism showed that the initial amounts of SDBS played a key role in the hollow structure formation; furthermore, a plausible mechanism based on a

micelle-assisted Ostwald ripening process was proposed. The prepared hollow magnetite spheres exhibit superparamagnetism in nature with a high saturation magnetization of 109.48 emu/g at 300 K. In addition, Cr (VI) ions adsorption data of magnetite hollow microspheres fit well with the Freundlich and Langmuir isotherm models correspond to the low and high Cr (VI) ions concentrations, respectively. By the analysis of the X-ray photoelectron spectrum of the product, the Cr (VI) uptake onto these synthesized magnetite hollow spheres was identified as a physicochemical process, including an electrostatic attraction followed by a redox process in which Cr (VI) was reduced into Cr (III).

■ ASSOCIATED CONTENT

Supporting Information

XPS spectrum of magnetite hollow spheres, FT-IR spectra of standard SDBS and typical magnetite sample, XRD patterns of the products obtained at different reaction times, UV−vis absorbance spectra of SDBS ethylene glycol solution with different concentration, effect of time on Cr (VI) removal by magnetite hollow spheres, XRD pattern and XPS spectrum of Cr (VI)-loaded magnetite hollow spheres, Langmuir and Freundlich isothermal parameters for Cr (VI) adsorption on Fe_3O_4 hollow microspheres and the error limits on data. This material is available free of charge via the Internet at http://pubs.acs.org/.

■ AUTHOR INFORMATION

Corresponding Author

*E-mail: smzhou@henu.edu.cn. Tel:+86-378-2868833-3712. Fax: +86-378-3881358.

Notes

The authors declare no competing financial interest.

■ ACKNOWLEDGMENTS

This study was partially supported by the Program for Science & Technology Innovation Talents in Universities of Henan Province (2008 HASTIT002) and by the Natural Science Foundation of China under Grants 20971036 and 51102077, and the Construct Program of the Key Discipline in Hunan Province (2011-76).

■ REFERENCES

(1) Park, H. J.; Tavlarides, L. L. *Ind. Eng. Chem. Res.* **2008**, *47*, 3401−3409.
(2) Wang, Y. Q.; Zou, B. F.; Gao, T.; Wu, X. P.; Lou, S. Y.; Zhou, S. M. *J. Mater. Chem.* **2012**, *22*, 9034−9040.
(3) Hu, J.; Lo, I. M.; Chen, G. *Water Sci. Technol.* **2004**, *50*, 139−146.
(4) Dean, J. G.; Bosqui, F. L.; Lanouette, K. H. *Environ. Sci. Technol.* **1972**, *6*, 518−522.
(5) Patterson, R. R.; Fendorf, S. *Environ. Sci. Technol.* **1997**, *31*, 2039−2044.
(6) Pettine, M.; Ottone, L. D.; Campanella, L.; Millero, F. J.; Passino, R. *Geochim. Cosmochim. Ac.* **1998**, *62*, 1509−1519.
(7) Yuan, P.; Liu, D.; Fan, M.; Yang, D.; Zhu, R.; Ge, F.; Zhu, J. X.; He, H. P. *J. Hazard. Mater.* **2010**, *173*, 614−621.
(8) Liu, B. H.; Han, M. Y.; Guan, G. J.; Wang, S. H.; Liu, R. Y.; Zhang, Z. P. *J. Phys. Chem. C* **2011**, *35*, 17320−17327.
(9) Zhu, J. H.; Wei, S. Y .; Gu, H. B.; Rapole, S. B.; Wang, Q.; Luo, Z. P.; Haldolaarachchige, N.; Young, D. P.; Guo, Z. H. *Environ. Sci. Technol.* **2012**, *46*, 977−985.
(10) Zhang, Y. X.; Xu, S. C.; Luo, Y. Y.; Pan, S. S.; Ding, H. L.; Li, G. H. *J. Mater. Chem.* **2011**, *21*, 3664−3671.
(11) Xuan, S. H.; Wang, F.; Lai, J. M. Y.; Sham, K. W. Y.; Wang, Y. X. J.; Lee, S. F.; Yu, J. C.; Cheng, C. H. K.; Leung, K. C. F. *ACS Appl. Mater. Interface* **2011**, *3*, 237−244.
(12) Chen, J. S.; Zhang, Y. M.; Lou, X. W. *ACS Appl. Mater. Interface* **2011**, *3*, 3276−3279.
(13) Kong, L. R.; Lu, X. F.; Bian, X. J.; Zhang, W. J.; Wang, C. *ACS Appl. Mater. Interface* **2011**, *3*, 35−42.
(14) Bao, N. Z.; Shen, L. M.; Wang, Y. H.; Ma, J. X.; Mazumdar, D.; Gupta, A. *J. Am. Chem. Soc.* **2009**, *131*, 12900−12901.
(15) Yuan, H. L.; Wang, Y. Q.; Zhou, S. M.; Liu, L. S.; Chen, X. L.; Lou, S. Y.; Yuan, R. J.; Hao, Y. M.; Li, N. *Nanoscale Res. Lett.* **2010**, *5*, 1817−1821.
(16) Yuan, H. L.; Wang, Y. Q.; Zhou, S. M.; Lou, S. Y. *Chem. Eng. J* **2011**, *175*, 555−560.
(17) Qiu, S. R.; Lai, H. F.; Roberson, M. J.; Hunt, M. L.; Amrhein, C.; Giancarlo, L. C.; Flynn, G. W.; Yarmoff, J. A. *Langmuir* **2000**, *16*, 2230−2236.
(18) Yu, B. Y.; Kwak, S. Y. *J. Mater. Chem.* **2010**, *20*, 8320−8328.
(19) Deng, H.; Li, X. L.; Peng, Q.; Wang, X.; Chen, J. P.; Li, Y. D. *Angew. Chem., Int. Ed.* **2005**, *44*, 2782−2785.
(20) Zhong, L. S.; Hu, J. S.; Liang, H. P.; Cao, A. M.; Song, W. G.; Wan, L. J. *Adv. Mater.* **2006**, *18*, 2426−2431.
(21) Sun, Q.; Ren, Z.; Chen, W. M.; Wang, R. M.; Chen, C. P. *J. Nanopart. Res.* **2010**, *13*, 213−220.
(22) Sun, Y.; Xia, Y. *Science* **2002**, *298*, 2176−2179.
(23) Wang, F. L.; Liu, J. R.; Kong, J.; Zhang, Z. J.; Wang, X. Z.; Itoh, M.; Machida, K. I. *J. Mater. Chem.* **2011**, *21*, 4314−4320.
(24) Hu, P.; Yu, L. J.; Zuo, A.; Guo, C. Y.; Yuan, F. L. *J. Phys. Chem. C* **2009**, *113*, 900−906.
(25) Sun, Q.; Ren, Z.; Chen, W. M.; Wang, R. M.; Chen, C. P. *J. Nanopart. Res.* **2010**, *13*, 213−220.
(26) Zhu, L. P.; Xiao, H. M.; Zhang, W. D.; Yang, G.; Fu, S. Y. *Cryst. Growth Des.* **2008**, *8*, 957−963.
(27) Luo, B.; Xu, S.; Ma, W. F.; Wang, W. R.; Wang, S. L.; Guo, J.; Yang, W. L.; Hu, J. H.; Wang, C. C. *J. Mater. Chem.* **2010**, *20*, 7107−7113.
(28) Jia, B. P.; Gao, L. *J. Phys. Chem. C* **2008**, *112*, 666−671.
(29) Wang, J.; Xu, H. F.; Zhang, H. J.; Song, J. W.; Gao, B. L; Huang, Y. D. *J. Mater. Sci.* **2011**, *46*, 2955−2962.
(30) Wang, X. Z.; Zhao, Z. B.; Qu, J. Y.; Wang, Z. Y.; Qiu, J. H. *Cryst. Growth Des.* **2010**, *10*, 2863−2869.
(31) Yu, D. B.; Sun, X. Q.; Zou, J. W.; Wang, Z. R.; Wang, F.; Tang, K. *J. Phys. Chem B* **2006**, *110*, 21667−21671.
(32) Lu, X. Y.; Jiang, Y.; Cui, X. H.; Mao, S. Z.; Liu, M. L.; Du, Y. R. *Acta Phys-Chem. Sin.* **2009**, *25*, 1357−1361.
(33) Liu, W.; Cholli, A. L.; Nagarajan, R.; Kumar, J.; Tripathy, S.; Bruno, F. F.; Samuelson, L. *J. Am. Chem. Soc.* **1999**, *121*, 11345−11355.
(34) Hait, S. K.; Majhi, P. R.; Blume, A.; Moulik, S. P. *J. Phys. Chem. B* **2003**, *107*, 3650−3658.
(35) Yiwei, T.; Zhuang, Z. B.; Peng, Q.; Li, Y. D. *Chem. Mater.* **2008**, *20*, 5029−5034.
(36) Cheng, W.; Tang, K. B.; Qi, Y. X.; Sheng, J.; Liu, Z. P. *J. Mater. Chem.* **2010**, *20*, 1799−1805.
(37) Deng, H.; Li, X. L; Peng, Q.; Wang, X.; Chen, J. P.; Li, Y. D. *Angew. Chem., Int. Ed.* **2005**, *44*, 2782−2785.
(38) Tan, Y. W.; Zhuang, Z. B.; Peng, Q.; Li, Y. D. *Chem. Mater.* **2008**, *20*, 5029−5034.
(39) Guardia, P.; Labarta, A.; Batlle, X. *J. Phys. Chem. C* **2011**, *115*, 390−396.
(40) Cao, C. Y.; Cui, Z. M.; Chen, C. Q.; Song, W. G.; Cai, W. *J. Phys. Chem. C* **2010**, *114*, 9865−9870.
(41) Guo, L. M.; Li, J. T.; Zhang, L. X.; Li, J. B.; Li, Y. S.; Yu, C. C.; Shi, J. L.; Ruan, M. L.; Feng, J. W. *J. Mater. Chem.* **2008**, *18*, 2733−2738.
(42) Huang, S. H.; Chen, D. H. *J. Hazard. Mater.* **2009**, *163*, 174−179.
(43) Yean, S.; Cong, L. *J. Mater. Res.* **2005**, *20*, 3255−3264.

(44) Dixit, S.; Hering, J. G. *Environ. Sci. Technol.* **2003**, *37*, 4182−4189.
(45) Hu, J.; Chen, G. H.; Lo, I. M. C. *Water Res.* **2005**, *39*, 4528−4536.